CBN 08-2

EVALUATION OF THE LOW COST COMPACT PPM PLANAR UNDULATOR MODEL *

Alexander B. Temnykh†, CESR-LEPP, Ithaca, New York, USA

March 4, 2008

Keywords:

Demagnetization; Magnetic field; NdFeB magnet; Undulator;

Abstract

To evaluate a number of ideas, which, in principal, can be implemented in the ERL insertion devices design, we built and tested 30cm long pure permanent magnet (PPM) undulator model. The model had $25.4mm$ undulator period, $5mm$ fixed gap and $\sim 1.07T$ maximum peak field on the beam axes. For the field strength control was utilized the phase adjustment scheme in which magnetic arrays are moved longitudinal with respect to each other. Magnetic arrays consisted of $NdFeB$ rectangular magnet blocks delivered "off the shelf" by Stanford Magnet Company. The model magnetic field was adjusted

*Work supported by the National Science Foundation under contract PHY 0202078

†Mail send to: A. Temnykh, Wilson Lab, Cornell University, NY 14850, USA. Tel. +1 607 255 4882, fax +1 607 255 8062, e-mail abt6@cornell.edu

to the level corresponding to $\sim 3.6^0$ of RMS undulator optical errors. For "zero" emittance beam these errors would cause reduction of the x-ray brilliance by $\sim 1\%$ at first, $\sim 3\%$ at third and $\sim 5\%$ at fifth harmonics, if compared with no-errors field.

The use "off the shelf" magnets and implementation of the phase adjustment scheme for the field control significantly reduced the cost and made design very compact without compromising operating properties.

In supplemental work one of the magnetic arrays was taken through the UHV cleaning procedure. With precautions, it was baked in vacuum at 120^0C for 48 hours. Measurements made after baking show acceptable out-gasing rate and no magnetic field change due to temperature demagnetization. This ensureds the capability of in-vacuum operation.

The paper describes the model mechanical design, magnetic field modeling and stress analysis, as well as properties of permanent magnet material used in the model and characteristics of the "off the shelf" permanent magnet blocks. It also reports results of the magnetic field measurement and tuning.

1 INTRODUCTION

A majority of the beam lines operating at synchrotron radiation (SR) facilities use radiation generated by permanent magnet (PM) undulator magnets. Because of the various requirements on synchrotron radiation properties there were developed and built many types of undulators. Independent of type, to provide efficient operation these magnets should have high magnetic field uniformity and precise field strength control.

Traditionally, to ensure the field uniformity undulator magnet builders request from PM manufacturers a special control on permanent magnets properties. In fact, this request considerably increases the cost of the magnets. In addition, because most of PM undulator utilize a field control scheme based on gap adjustment, they requires large rigid movable mechanical structures that should withstand strong magnetic forces and provide precise motion. Usually these structures are very massive, take a lot of space and are quite expensive. As a result, the cost of the undulator magnets of traditional design reach $\sim 1.0M$ dollars per meter of structure or even more. The high

cost and the need for the space often impose limitations on the experimental capabilities.

In undulator model described below we used "off the shelf" PM blocks (after proper sorting) and the field control mechanism based on a phase adjustment (PA) concept developed and tested by Roger Carr, see references [2] and [3]. These considerably reduced the cost and made the design very compact without magnetic field quality compromise. The model can be easily scaled to a longer device.

2 Design considerations

The magnetic array design is illustrated on Figures 1. It is different from the traditional one.

The stack of the rectangular magnets consists of horizontally and vertically magnetized ("H" and "V") blocks that are attached to the base plate using two common for all block holders as shown in Fig. 1. To provide rigidity, two stabilizing bars are bolted to the base from the opposite side. Dimensions of the stabilizing bars were chosen from a stress analysis, see section 4.

The field tuning mechanism is the following. In the course of the design study it was noticed that the net magnetic force acting on "H" blocks in the magnet assembly always pushes the blocks away from the gap, while the forces acting on "V" blocks push blocks in the direction of the gap, see schematic in Fig. 2. This feature was utilized in the field adjusting mechanism. Two bars holding magnets have rectangular slots with vertical dimension larger, by $\sim 0.75mm$, than the magnetic block height. This provides space for magnet vertical displacement that is used for magnetic field tuning. In the tuning process, "H" blocks were pushed up by set-screws (1) coming from the base plate. To provide adjustment in both directions in the beginning of tuning procedure all "H" blocks were pushed half way up. Vertical magnetized blocks were displaced (pushed down) by inserting a thin stainless steel shim (2) between holder lip and magnet as illustrated on Figure 2.

In longitudinal direction magnet blocks stack to each other. Thus, the block positioning depends on thickness and the dispersion in thickness translates into period variation and, consequently, to undulator optical phase errors. Fortunately, this type of the phase errors can be easily corrected by the

vertical displacement of horizontal magnetized blocks, see discussion in the following sections.

The whole model assembly is depicted in Fig. 3. The model consists of upper and lower magnetic rows (1). Four miniature rails NSK LU09AR (2) specified for up to $1770N$ static load with $\sim 2in$ stroke were placed between the rows. The rails provided smooth longitudinal displacement of one row relative to another. For rows shift we used a single steel bolt with nuts pressing against two grips (3), as seen in Fig. 3. The assembly can be fitted into a round $18cm$ ID pipe.

3 Magnetic field modeling

For magnetic field calculation we use 3D magnetic modeling software [4]. One example of the software output is depicted in Figure 4. It shows a 3D view of one undulator period with a contour plot of vertical magnetic field in the middle plane. Calculation predicted $1.08T$ peak field and $110N/period$ or $1300N$ of total attractive force between rows for "zero" displacement between them. As was pointed out in [3], the vector of net magnetic force rotates with the row displacement. For 1/4 period displacement, 90^0 of the phase shift, the force is horizontal, at 180^0 phase magnetic rows are repelling each other. The magnitude of the force is independent of phase. In the tested model four miniature rails NSK LU09AR specified for $1700N$ static load provided a smooth row shifting with safety factor more than 4.

Fig. 5 shows vertical and longitudinal magnetic field profiles on beam axis for one period for "zero" (a) and for $10.35mm(140^0)$ (b) shifts between rows. It indicates the appearance of a longitudinal field with amplitude comparable with the main field. A more detailed picture of the field can be seen in Fig. 6 and 7.

Detailed analysis of the magnetic field properties for an adjustable phase type undulator has been done in references [2], [3]. There it was found that when compared to a conventional adjustable gap (AG) device, the AP scheme provides:

- Independence of field integrals on phase shift between magnet rows.
- Constant vertical focusing effect with phase variation.

These features obviously make the AP design superior. However, the problem of magnetic stress, see discussion below, may impose limitations on AP type undulator application.

Fig. 6 depicts magnetic field lines for $5mm$ gap and "zero" shift between magnetic rows. Here vertical peak field $\sim 1.06T$ and minimum field in horizontaly magnetized blocks $\sim 0.18T$. The latter corresponds to 107^0C of demagnetizing temperature, see temperature demagnetization data in section 5.

Fig. 7 shows field lines for $5mm$ gap and $10mm$ (144^0) shift between magnetic rows. The shift resulted in reduction of the vertical peak field to $\sim 0.28T$. In this configuration the H-block minimum field will be $\sim -0.27T$. The negative sign means the field direction is opposite to magnetization. Using the temperature demagnetization data, see Fig. 10, one can estimate a demagnetization temperature as $\sim 55^0C$.

In the AG scheme, field is controlled by changing gap as shown in Fig. 8. There we have depicted magnetic field lines for $17mm$ gap and "in phase" magnetic rows. Under this conditions, maximum vertical magnetic field is similar to the previous, $\sim 0.27T$, while the minimum field in H-block is larger $\sim -0.05T$. The latter result suggests less magnetic stress. According to the temperature demagnetization data, the $-0.05T$ field results in $\sim 80^0C$ of demagnetizing temperature, which is 25^0C higher than for AP scheme.

This example shows that in application with risk of significant temperature rise, the adjustable gap scheme for the field control could be more suitable.

4 Stress analysis

Stress analysis has been done using Autodesk Inventor software. Two pictures showing the model deformation for "in phase" rows position and for 90^0 shift are depicted in Fig. 11.

In the first case, $1300N$ of the magnetic forces, see section 3, were applied to the holders in vertical direction while the rails horizontal surfaces were constrained against vertical motion. It resulted in $\sim 10\mu m$ maximum deformation in the middle, see Fig.11 top, which can be considered as acceptable. Without stabilizing bars deformation would be much bigger.

The bottom plot in Fig. 11 depicts deformation at 90^0 shift between

rows. In this case the net magnetic force vector is in horizontal plane. In the calculation, $1300N$ horizontal force was applied to the holders while constrain was applied to the piece called "grip". The resulting deformation was found to be $\sim 4\mu m$ which is acceptable.

At 180^0 shift magnetic forces will repulse the rows from each other. The deformation will be similar to shown in Fig. 11 (top), but of opposite sign.

5 Permanent magnet material properties

Magnetic arrays were assembled with rectangular NdFeB permanent magnet (PM) blocks of $1.0 \times 0.5 \times 0.25$" dimensions plated by $\sim 10\mu m$ layer of $Cu - Ni$. The PM material magnetic properties are depicted in the Table 1.

$Grade$	$\frac{Br}{(KGs)}$	$\frac{Hc}{(KOe)}$	$\frac{Hci}{(KOe)}$	$\frac{(BH)max}{(MGOe)}$
$N40SH$	12.4-12.8	≥ 11.8	≥ 20	38-41

Table 1: Characteristics of the used NdFeB PM materials

For the assembly 96 blocks were used. Half were magnetized in the 0.5" direction, the rest in the 0.25". First type of magnet is referred as a "V"-blocks, the second type as "H"-blocks. The magnets were ordered from Stanford Magnet Company and were delivered within 5 weeks at a price ~ 3 dollars per block.

Demagnetizing characteristics are shown in Fig. 9 and 10. Fig. 9 depicts demagnetization curves for $NdFeB$ permanent magnetic material of $N40SH$ grade at different temperature. Here vertical scales are intrinsic magnetic field in direction of magnetization and specific magnetic moment, horizontal is magnetic field induction applied in direction opposite to magnetization. Knees seen in curves indicate points of irreversible demagnetization. For example, 120^0C curve indicates that PM material will be irreversible demagnetized if 7.8kOe are applied in the opposite to magnetization direction. The intrinsic magnetic field under this conditions will be $\sim 3800G$, see right scale. This is a minimum of the intrinsic field which can be reached without irreversible demagnetization at 120^0C of temperature.

Dependence of minimum magnetic field on temperature was extracted from data depicted in Fig. 9 and plotted in Fig. 10. The linear fit for the temperature dependence on the field gives:

$$T_{demag}[^0C] = 86.52 + 0.0115 \times B_{min}[G] \quad (1)$$

6 PM blocks characterization and sorting

Before assembly PM blocks were characterized and sorted. Magnetic moments and direction of magnetization were measured using Helmholtz coils and the blocks thickness was measured with precise caliper.

Following the magnetic measurements, $\sim 10\%$ of the magnets with the biggest deviation from mean value were excluded from the pool. After that the dispersion in magnetic moments of the remaining magnets had $(\triangle M/M)RMS \sim 0.4\%$, see histograms *a*) and *b*) in Fig. 12. These magnets were then sorted according to their strength and their positions in assembly were optimized to maximize field uniformity.

Special attention was paid to errors in magnetization direction of "V" blocks. If magnetization and consequently magnetic field have a horizontal component, there will be the beam trajectory distortion in vertical plane, which would be difficult to compensate. Histogram depicted plot *c*) in Fig. 12 indicates a $0.68^0(1.9mrad)$ RMS of deviation magnetization direction. This translates into $\sim 4.75G$ of the RMS random horizontal field component on beam axis or into $0.2\mu rad$ random vertical kicks for $5GeV$ electron beam. The beam vertical trajectory walk out rate due to these kicks will be $dy[\mu m] \simeq 0.02 \times \sqrt{L_u[m]}$, where L_u is the assembly length. For any reasonable length it is negligible.

The RMS deviation of the block thickness, see plot *d*) on Fig. 12 was found to be $\sim 30\mu m$, which corresponds to $\sim 60\mu m$ of the period variation. Assuming 360^0 optical phase advance per period (first harmonics) and $25.4mm$ period one can estimate the RMS optical phase errors due to variation in block thickness as 0.85^0. These errors are small and can be easily compensated by "H"-blocks vertical position adjustment, see next section.

7 Magnetic field measurement and tuning

For magnetic field measurement we used Lake Shore Model 455 DSP Gaussmeter with Hall probe HST-4. In our setup the Hall probe was fixed while the undulator model sitting on a linear stage was moved in $\sim 0.25mm$ steps. The typical field scan consisted of ~ 1500 steps and took ~ 5 minutes. The stage motion and magnetic field data collection were controlled by laptop "IBM-T42" with program based on LabView software. For data analysis we used B2E package version 3.3 developed by ESRF ID Group [1].

Plots on Fig. 13 and 14 depict magnetic field profile, trajectory and optical phase errors before and after magnetic field tuning.

The field measurement before tuning reveal the peak field $\sim 1.067T$ and the peak field deviation $dB_{peak}/B \simeq 0.6\%$. Both are close to expected. The data analysis indicated satisfactory trajectory, see Fig. 13 (b), and optical phase errors (RMS) $\sim 5.5^0$, see dashed line in Fig. 14. Taking into account the simplicity of the model design and the fact, that magnet used in the model were delivered off the shelf, the field quality and phase errors can be considered as remarkable.

The field tuning procedure consisted of a number of iterations of the field measurement, data analysis, and magnet displacements. The main goal was to reduce optical phase errors while keeping the beam trajectory satisfactory. The field correction was done by small displacements of the "H" and "V" magnets using the mechanism described in section 2.

Plots on Fig. 15 show the measured local magnetic field change on the beam axis caused by $0.25mm$ displacement of single "H" and "V" blocks, and corresponding change in beam trajectory and optical phase.

One can see that "H" block displacement results in asymmetric magnetic field variation with amplitude $\sim 1.2\%$ of B_{max}, Fig. 15 (a). "V" block displacement causes symmetric field change with similar amplitude, Fig. 15 (b). Because of the profile difference, their effects on the beam trajectory and optical phase are quit different as indicated in the bottom plots on Fig. 15. "H" block displacement creates $\sim 0.05\mu m$ step in trajectory and $\sim 4^0$ step in the optical phase. This trajectory distortion in negligible in compare with $\pm 1\mu m$ trajectory wiggling caused by the main field. The optical phase change is significant.

"V" block displacement results in $\sim 0.85\mu rad$ trajectory deflection which for $300mm$ model length translates into $0.25\mu m$ (12.5% of the wiggleing

amplitude) trajectory offset and creates $\sim 2^0$ optical phase distortion.

The difference in the trajectory and optical phase responses for "H" and "V" blocks displacements suggests a simple field tuning strategy. First, one can correct trajectory by adjusting of "V" blocks positions, then correct optical phase with "H" blocks displacements.

In our case, because of satisfactory trajectory, the field tuning was done mostly by the "H" blocks position adjustment. One can notice that while plots in Fig. 13 indicated almost no difference in the field profile and in the beam trajectory before and after tuning, the difference in the optical phase errors is very pronounced, see Fig.14. The large $\sim 15^0$ local phase error in the vicinity of 12-th pole was completely tuned out, the RMS optical phase error was reduced from 5.5^0 to 3.3^0. This field tuning required 11 iterations and took $\sim 4hrs$.

It is interesting to note that the tuning increased RMS peak field from 0.6% to 0.9%. This means the field strength variation, in fact, compensated variations in the undulator period length.

After the field tuning was done, the field of the undulator model was measured at various shifts between magnet rows.

Results for 0^0 ("in phase" position), 92^0 and 141^0 shifts are plotted in Fig. 16. As one can expect the maximum peak field is for "in phase" position. For shifted rows the peak field is lower.

Fig. 17 shows spectrum of the photon flux through the $10\mu rad$ circular slit calculated by software "SPECTRA" [5] for ERL "High coherence" mode of operation and for field distribution measured at various phases between rows.

The arrows connecting peaks in spectrum show how undulator harmonics shift when phase is varied. From this plot one can see that the given model provides good overlap between harmonics and can be used for x-ray generation in range from $2keV$ to $20keV$. The field errors cause no more than a few percent flux degradation over the photon energy range.

8 Conclusion

We built and tested $30cm$ long model of PPM planar undulator with field control based on the shift of magnet rows relative to each other. The model was assembled from $NdFeB$ permanent magnets, had fixed $5mm$ gap, $25.4mm$

undulator period and 1.07 $Tesla$ maximum peak field on beam axes. In the course of the model design and building the following non-traditional approaches have been used:

- "Off the shelf" magnets were utilized. On one hand, these magnets are much cheaper than when made under high tolerance control and can be delivered in much shorter time, on the other hand, there was no assurance of their quality. Our experience has shown that with 10% of the magnets excluded, the rest satisfied the requirements usually required for undulator magnets.

- We used a simple magnet fastening scheme. It consisted of two holders common for all blocks with provision for magnet position adjustment. The scheme provided magnetic field tuning to a satisfactory level.

- We used a row shifting mechanism based on miniature rails placed between rows in the middle plane. This arrangement made the whole design compact enough to fit into $18cm$ ID round pipe.

It should be also noted that the design was optimized using 3D magnetic field modeling and stress analysis. The predicted model deformation does not exceed $10\mu m$. The residual magnetic field errors, left after field tuning, should cause no more than few percent of the x-ray flux degradation.

The model test demonstrated that one can design and built compact, low cost undulator magnet without compromising of the operating properties.

9 Acknowledgements

Author would like to thank David Rice, Sol Gruner, Don Bilderback and especially Ken Finkelstein for support, useful discussions and help.

References

[1] J. Chavanne, P. Elleaume, ESRF Internal Report ESRF-SR/ID-91-54.

[2] Roger Carr, Adjustable phase insertion device as X-ray sources, Nucl. Instr. And Meth. A 306 (1991) 391-396

[3] Roger Carr and Heinz-Dieter Nuhn, Design study for an adjustable phase undulator, Rev. Sci. Instrum. 63(1) (1991) 347-351

[4] VECTOR FIELDS software for electromagnetic design.

[5] T. Tanaka and H. Kitamura, J. Synchrotron Radiation 8(2001) 1221

[6] MAURER MAGNETIC AG, URL : *www.maurermagnetic.ch*

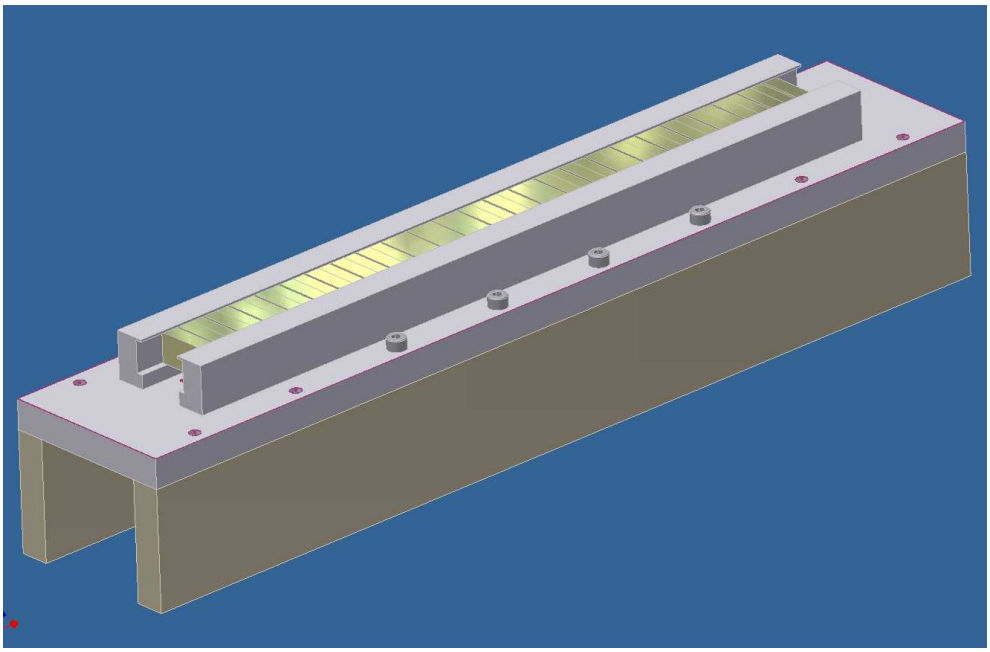

Figure 1: Magnetic array general view

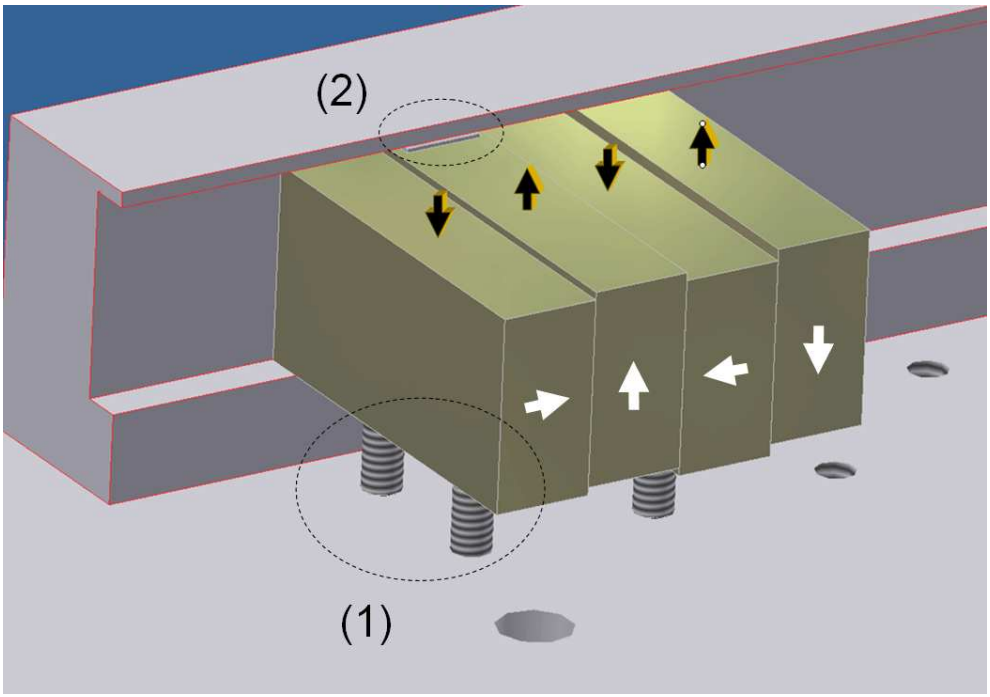

Figure 2: Field tuning mechanism. Arrows on the side indicate the magnetization direction. The top arrows show the net magnetic forces acting of the blocks. For the presented model they are $\sim 110N$ per magnet. (1) - set-screws used for "H" blocks displacement, (2) - stainless steel shim used for displacement of "V" block.

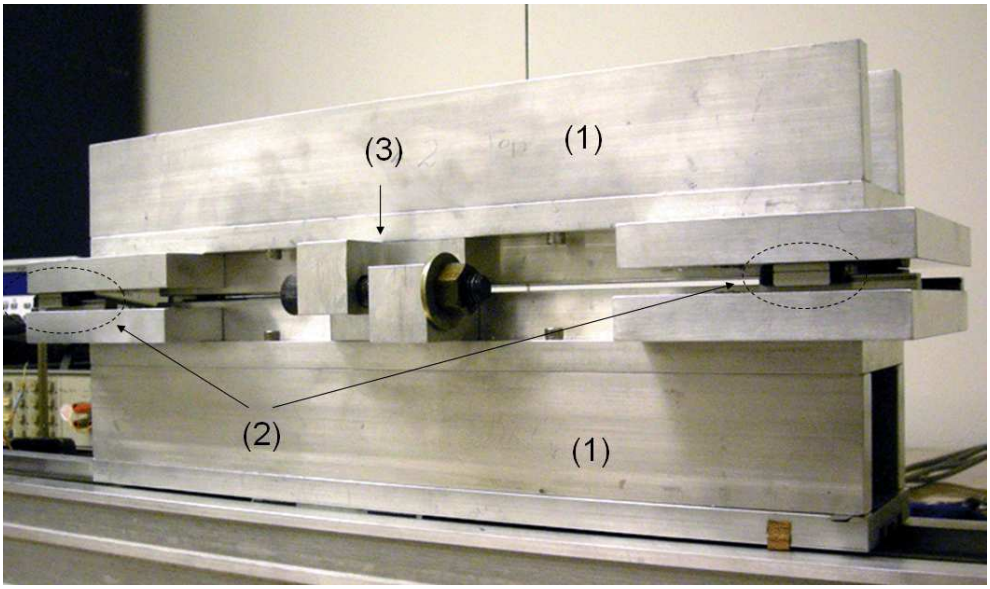

Figure 3: The model picture. (1) - magnet rows, (2) - miniature rails, (3) - row shifting mechanism

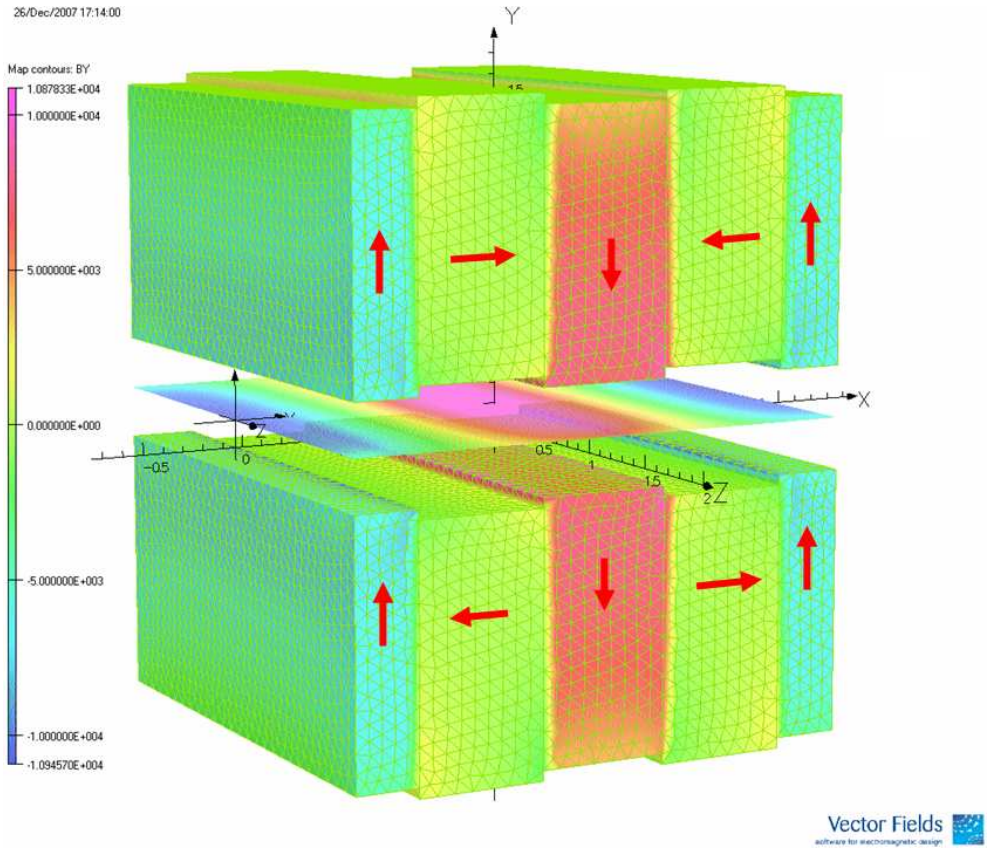

Figure 4: 3D magnetic modeling of one period of the undulator. Arrows indicate direction of the PM blocks magnetization

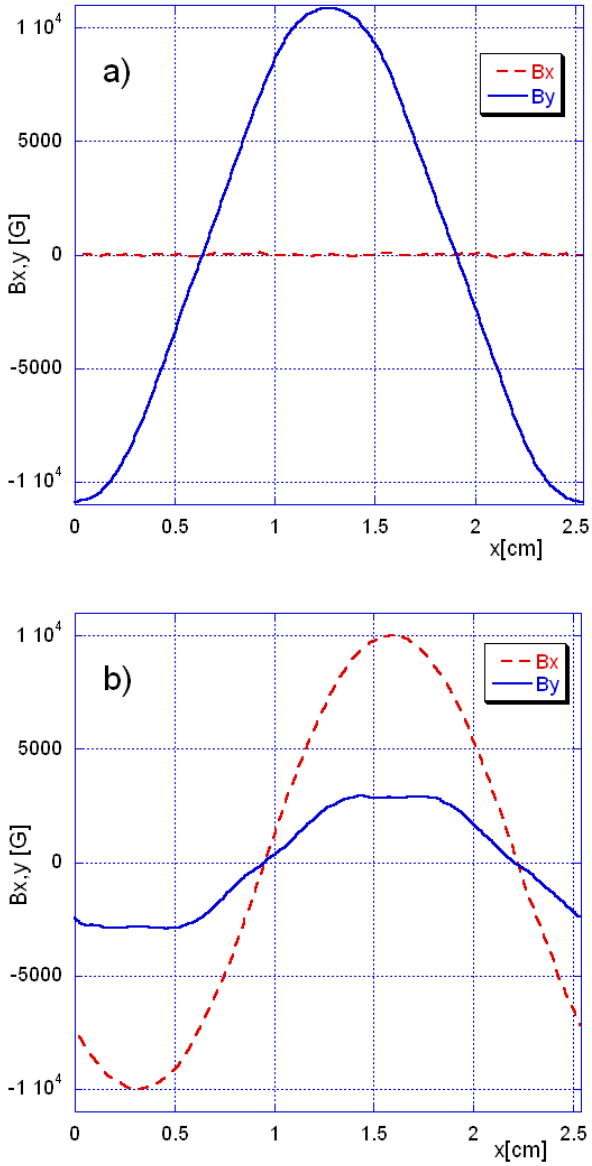

Figure 5: Vertical (solid line) and longitudinal (dashed line) magnetic fields on beam axis. a) No shift between magnetic rows, $B_{y,max} = 1.08T$, $B_{x,max} \simeq 0$. b) $10.35mm$ (140^0) shift between rows, $B_{y,max} = 0.29T$, $B_{x,max} = 1.00T$

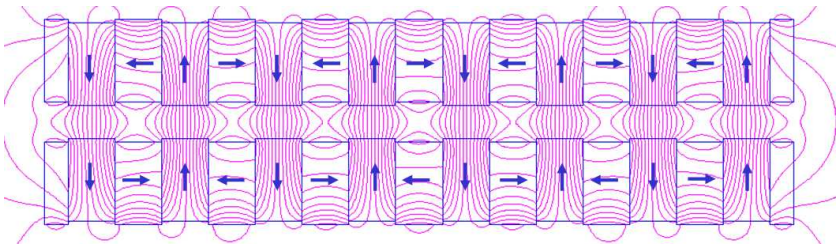

Figure 6: POISSON 2D calculation. Magnetic field lines for $5mm$ gap and "in phase" magnetic rows position. Vertical peak field on beam axis $\sim 1.06T$. In "H" blocks $B_{x,min} \sim 0.18T$, $T_{demag} = 107^0C$.

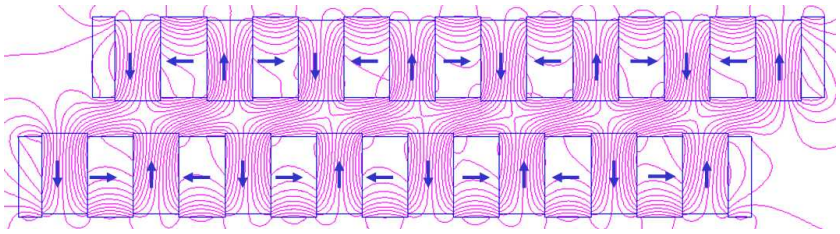

Figure 7: POISSON 2D calculation. Magnetic field lines for $5mm$ gap and 10mm (144^0) magnetic rows shift. Vertical peak field $\sim 0.27T$. In "H" blocks $B_{x,min} \sim -0.27T$, $T_{demag} = 55^0C$.

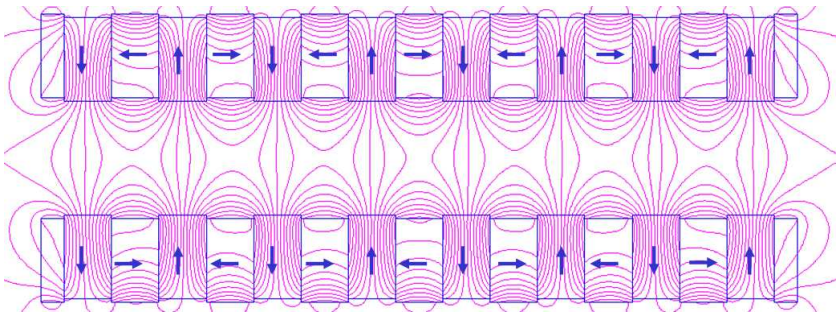

Figure 8: POISSON 2D calculation. Magnetic field lines for $17mm$ gap and "in phase" magnetic rows position. Vertical peak field on beam axis $\sim 0.27T$. In "H" blocks $B_{x,min} \sim -0.05T$, $T_{demag} = 80^0C$.

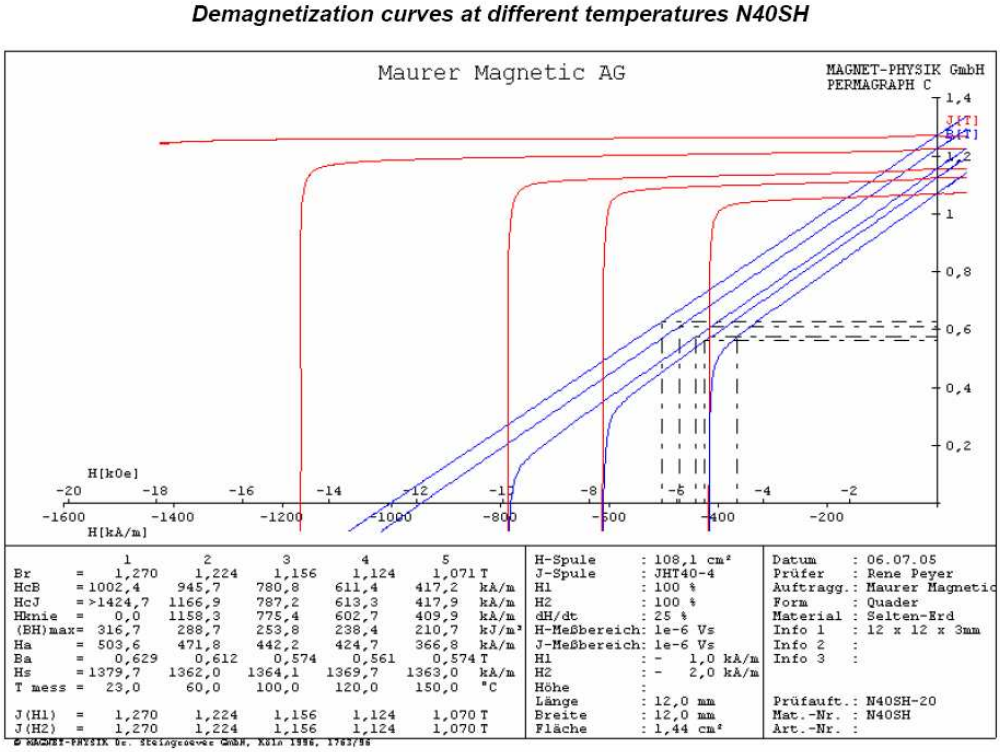

Figure 9: Demagnetization curves for different temperature for N40SH Nd-FeB permanent magnet material. The data was copied from MAURER MAGNETIC AG web site [6]

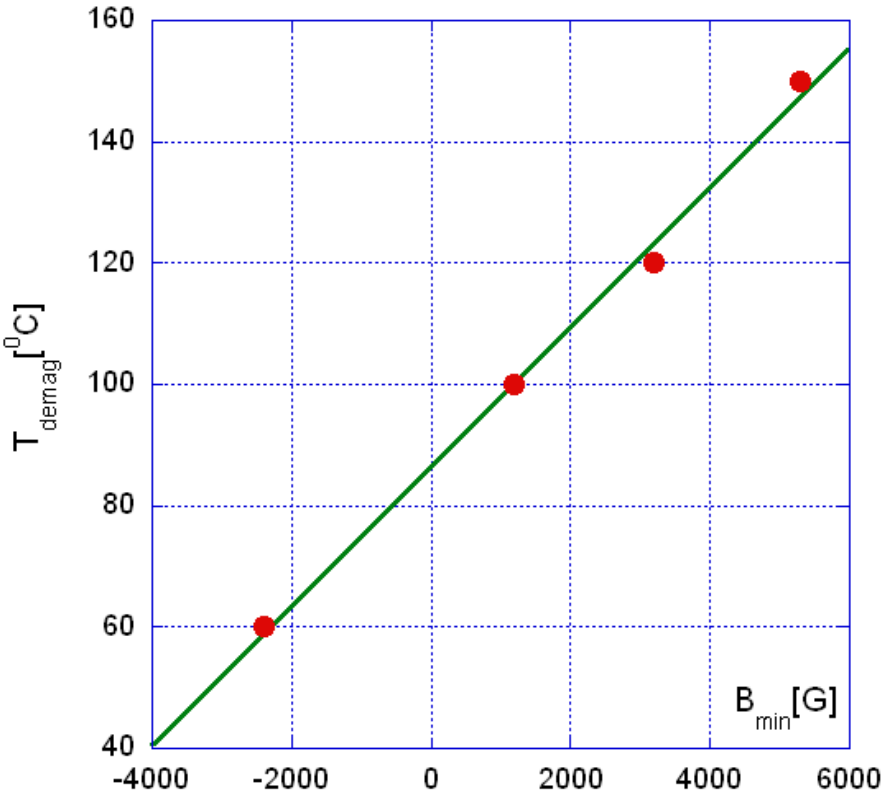

Figure 10: Demagnetizing temperature as a function of the minimum intrinsic field. The linear fit gives: $T_{demag}[^0C] = 86.52 + 0.0115 \times B_{min}[G]$

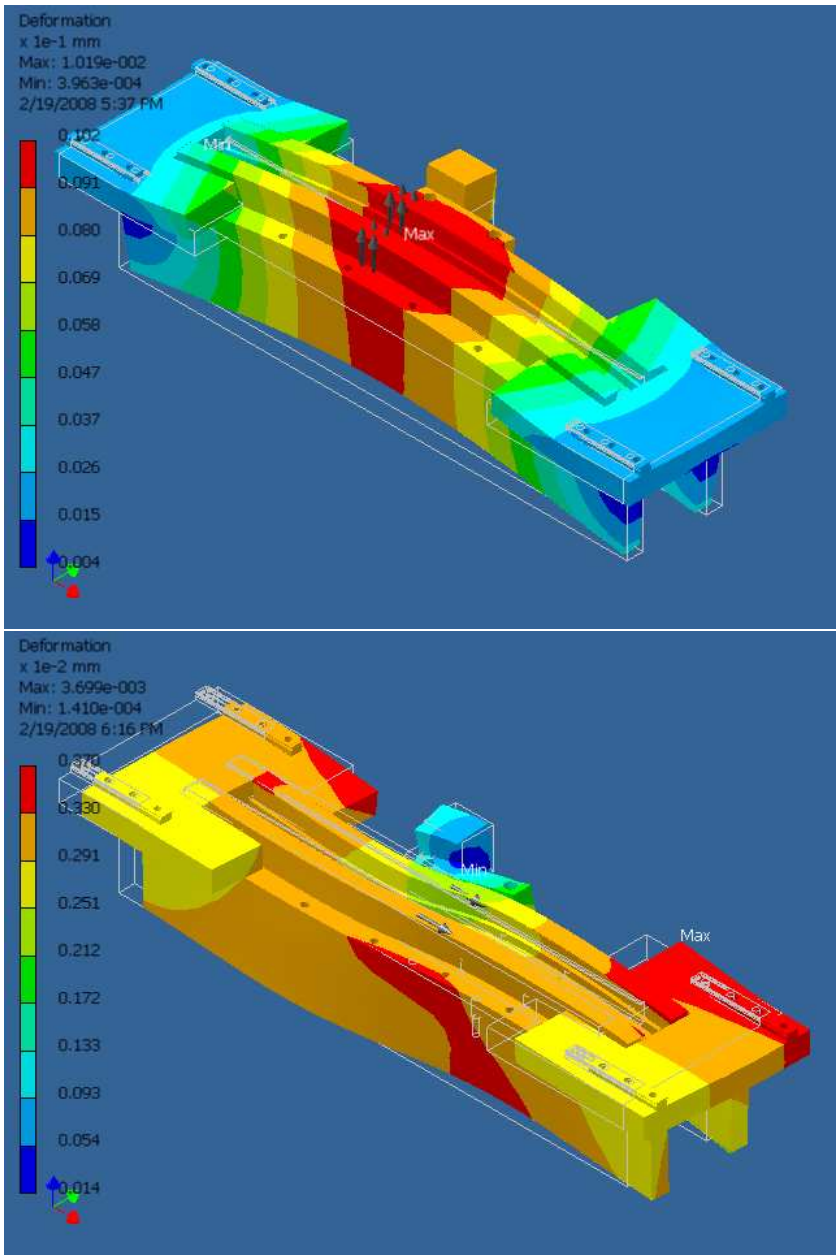

Figure 11: Deformation for "in phase" (top) and 90^0 shift (bottom) row positions. Maximum deformation for "in phase" position $\sim 10\mu m$, for 90^0 shift $\sim 4\mu m$

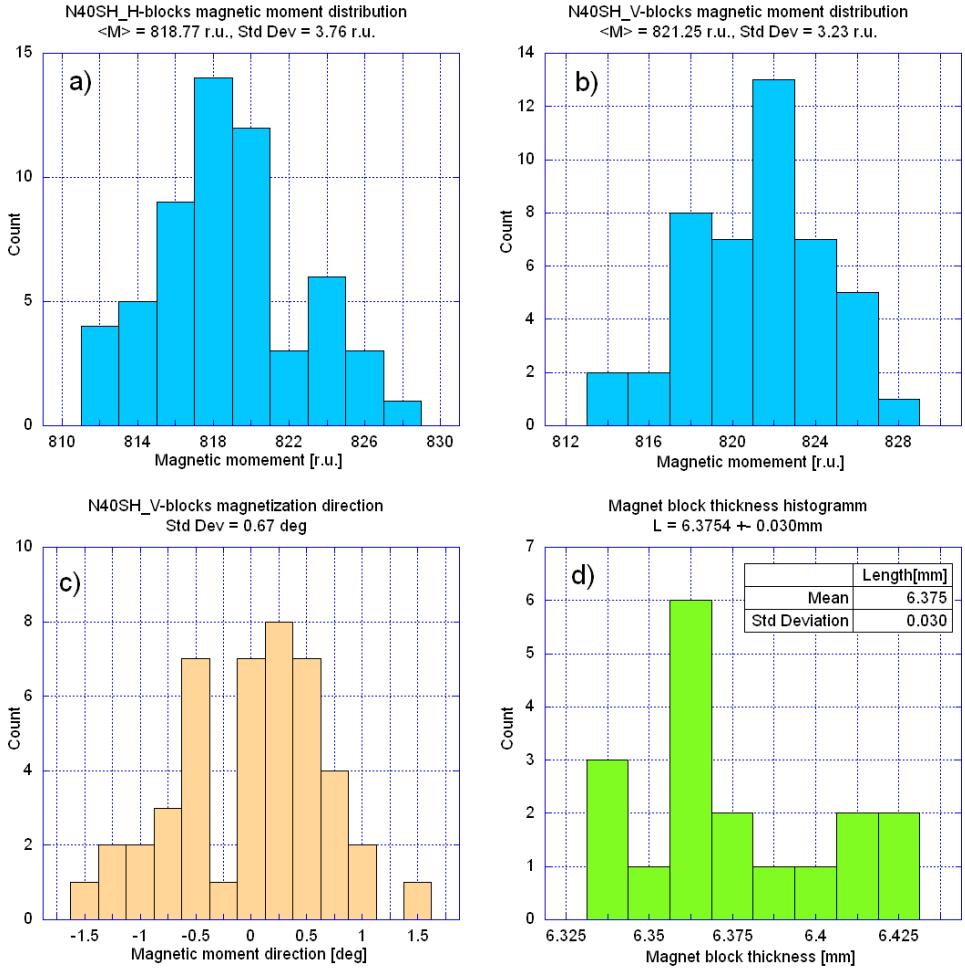

Figure 12: PM blocks characterization. a) "H" blok magnetic moment distribution, $(\triangle M/M)RMS \simeq 0.46\%$; b) "V" blok magnetic moment distribution, $(\triangle M/M)RMS \simeq 0.39\%$; c) Dispersion in the "V" - block magnetization directions $RMS \simeq 0.67^0$; d) The block thickness distribution $\triangle L$ RMS $\simeq 30\mu m$.

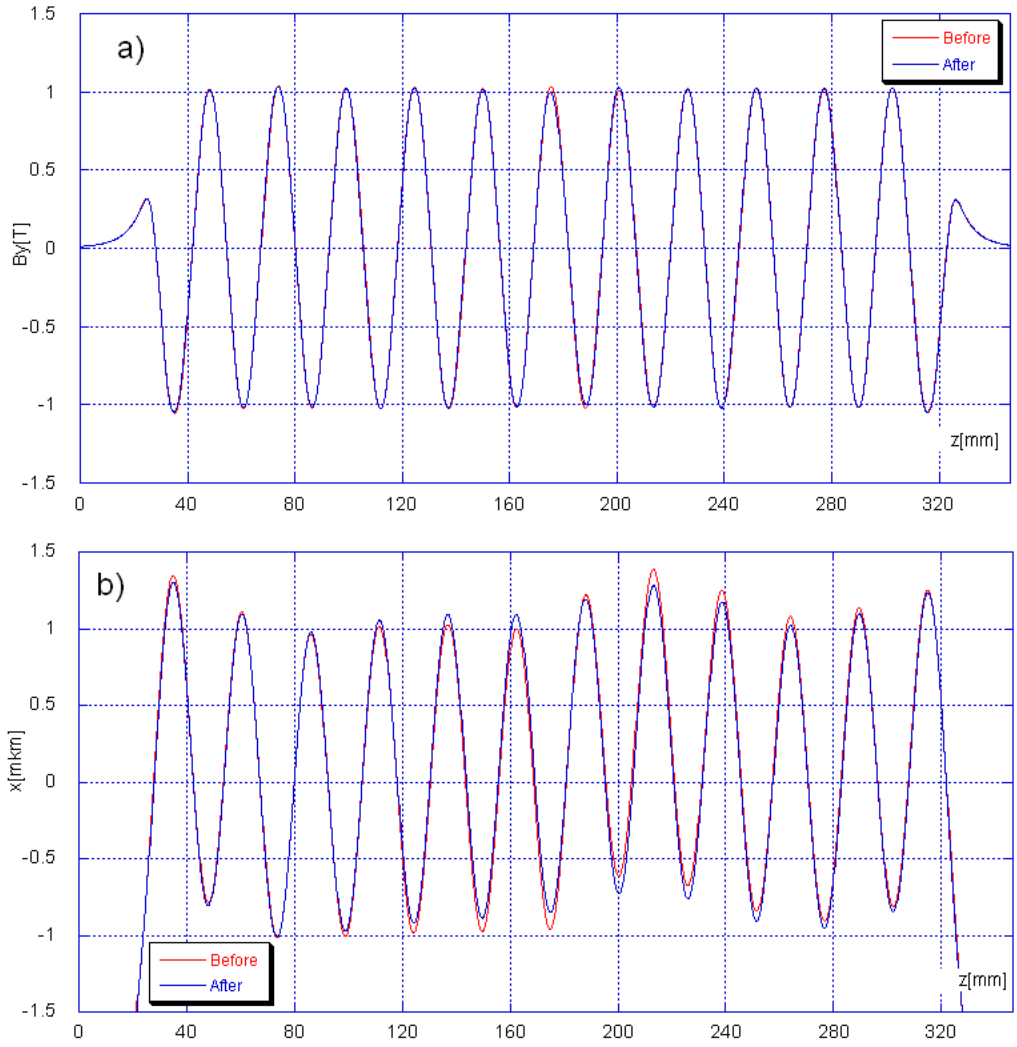

Figure 13: Measured magnetic field profile (a) and calculated beam trajectory (b) before and after tuning.

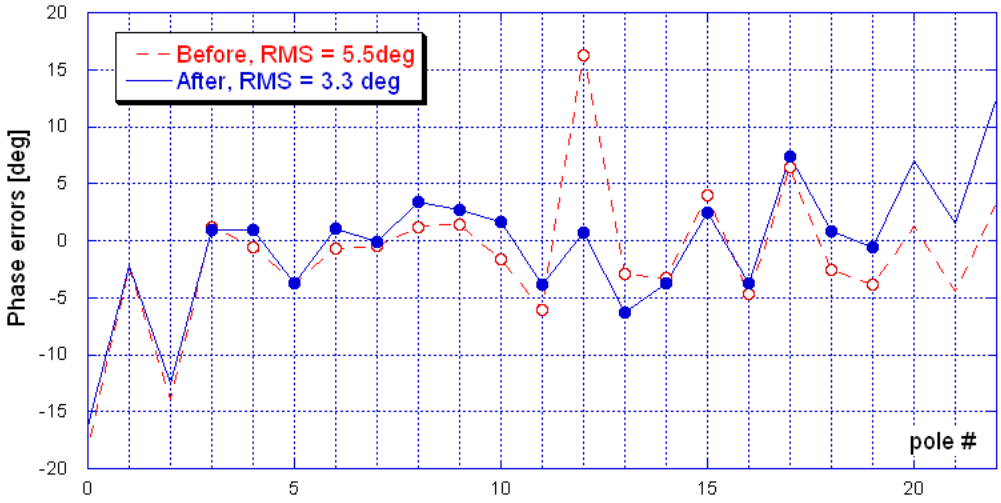

Figure 14: Optical phase errors before (dashed line) and after (solid line) tuning.

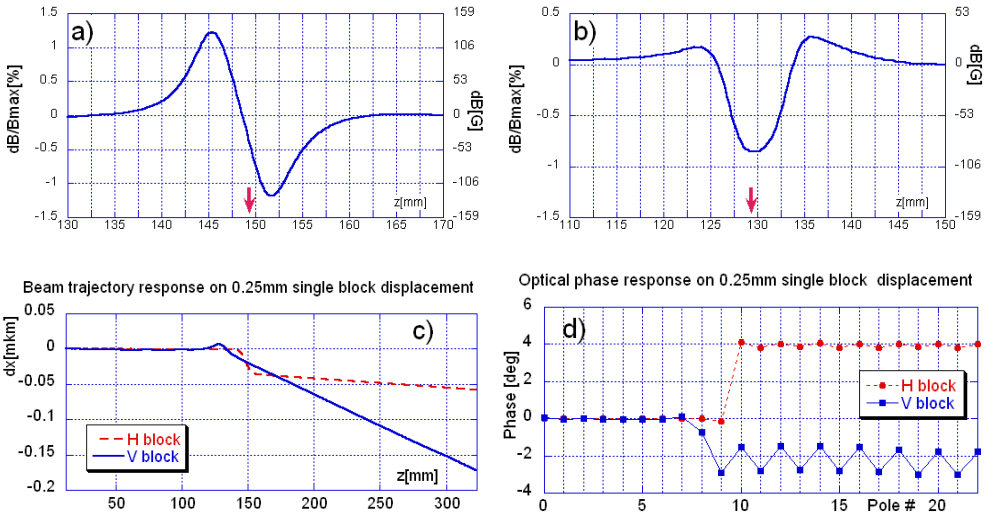

Figure 15: Top: magnetic field variation on the beam axis caused by $0.25mm$ of vertical displacement of "H" (left plot) and "V" (righ plot) blocks. Arrows indicate the block locations. Bottom: beam trajectories (left plot) and optical phases (right plot) changes corresponding to the field variation shown at top plots.

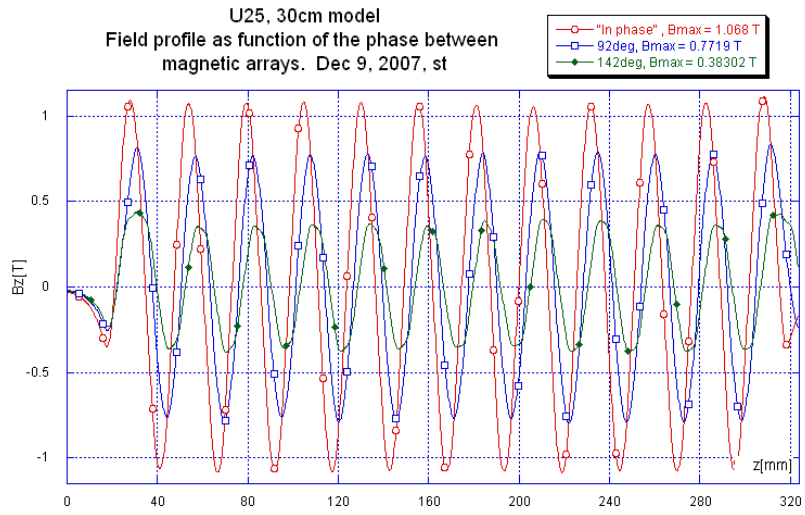

Figure 16: Field profile for various phase between magnetic rows.

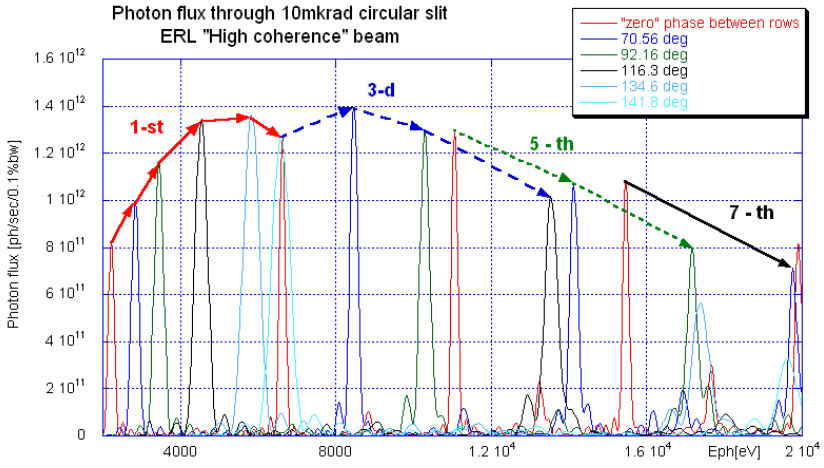

Figure 17: Spectrum of the photon flux for various phase between rows. Arrows show the undulator harmonics shift when phase varied.